Hindawi
Advances in Materials Science and Engineering
Volume 2019, Article ID 5809657, 13 pages
https://doi.org/10.1155/2019/5809657

Research Article

Research on the Dynamic Mechanical Properties and Energy Dissipation of Expansive Soil Stabilized by Fly Ash and Lime

Sheng-quan Zhou[1,2], **Da-wei Zhou**[1,2], **Yong-fei Zhang**[1,2], **Wei-jian Wang**[1,2] and **Dongwei Li**[3]

[1]*School of Civil Engineering and Architecture, Anhui University of Science and Technology, Huainan 232001, China*
[2]*National Engineering Laboratory for Deep Shaft Construction Technology in Coal Mine, Anhui University of Science and Technology, Huainan 232001, China*
[3]*School of Civil and Architectural Engineering, East China University of Technology, Nanchang 330013, China*

Correspondence should be addressed to Da-wei Zhou; 2997805549@qq.com

Received 11 September 2019; Accepted 2 November 2019; Published 6 December 2019

Academic Editor: Georgios I. Giannopoulos

To probe into the dynamic mechanical properties of expansive soil stabilized by fly ash and lime under impact load, the split-Hopkinson pressure bar (SHPB) test was carried out in this study. An analysis was made on the dynamic mechanical property and final fracture morphology of stabilized soil, and the failure mechanism was also explored from the perspective of energy dissipation. According to the test results, under the impact pressure of 0.2 MPa, plain soil and pure fly ash-stabilized soil exhibit strong plasticity. After the addition of lime, the stabilized soil shows obvious brittle failure. The dynamic compressive strength and absorbed energy of stabilized soil first increase and then decrease with the change of mix proportions. Both the dynamic compressive strength and the absorbed energy reach the peak value at the content of 20% fly ash and 5% lime (20% F + 5% L). In the process of the test, most of the incident energy is reflected back to the incident bar. The absorbed energy of stabilized soil increases linearly with the rise of dynamic compressive strength, while the absorbed energy is negatively correlated with the fractal dimension. The fractal dimension of pore morphology of the plain soil is lower than that of the fly ash-lime combined stabilized soil when it comes to the two different magnification ratios. The test results indicate that the modifier content of 20% F + 5% L can significantly improve the dynamic mechanical properties of the expansive soil.

1. Introduction

Expansive soil refers to a type of clay with repeated expansion and shrinkage properties in terms of its moisture variations [1–4]. Its main mineral components include montmorillonite and illite [5–9]. It was not until 1938 that the United States Reclamation Bureau initially discovered the problem caused by expansive soil in a foundation engineering project in Oregon. Since then, engineers have come to realize the damage of expansive soil causes to engineering. In recent years, a variety of methods have been explored by many scholars with the purpose of stabilizing expansive soil. The research results show that cement and lime [10], fly ash [11], etc., all prove to be effective materials to reduce the expansion potential of expansive soil.

Apart from exploring materials like fly ash and lime to reduce the expansion potential of expansive soil, the static mechanical properties of stabilized soil have also been explored comprehensively. The change laws of unconfined compressive strength [12–14], split tensile strength [12], and shear strength [14, 15] as well as other parameters of stabilized soil with different mix proportions have been obtained by relevant studies in order to acquire the optimal mix proportion of the modifier. Besides, the mechanism for the stabilization of expansive soil with fly ash and lime has been illustrated microscopically by some scholars [16, 17].

Based on the works above, abundant experience has been accumulated for the research and application of stabilized expansive soil. However, most of the research studies mainly focus on the quasi-static condition, and there are quite

limited studies on the dynamic mechanical properties of stabilized soil under impact load. In engineering practice, the stabilized expansive soil bears not only static load but also dynamic impact load. The stabilized expansive soil is usually used for the subgrade of the airport. When the aircraft is swept to the ground at high speed, it has a severe impact on the runway roadbed. Additionally, when mechanical excavation or blasting is conducted around the reinforced expansive soil foundation, dynamic impact on the foundation occurs. Moreover, impact loads such as earthquakes and vehicle vibration are also potential to affect the stability of the composite foundation [18, 19]. All the cases above involve the dynamic mechanical response of soil materials, and compared with the static mechanical properties, the dynamic mechanical properties of soil materials vary greatly. Therefore, it is of great significance to carry out research on the dynamic mechanical properties of stabilized soil under impact load.

It differs a lot between the dynamic and static mechanical properties of materials or structures, which is mainly reflected in two aspects: firstly, under the action of static loads, the solid medium is in a state of static equilibrium, in which the inertial action of the medium element can be neglected. However, the impact loads are characterized by a short duration of time, with the motion parameters changing significantly on a short time scale in milliseconds, microseconds, or even nanoseconds. Under the condition of such dynamic loads, the inertial properties of the medium microbody have to be considered. Secondly, the characteristics of the strong impact loads mean the motion parameters change significantly on the short time scale, which is sure to lead to a high strain rate. Generally, the strain rate in the conventional static test is on the order of $10^{-5}s^{-1}$~$10^{-1}s^{-1}$, while in the impact test, it is generally $10^{1}s^{-1}$~$10^{4}s^{-1}$ and even up to $10^{7}s^{-1}$, with many orders of magnitude higher than those in the static test. According to many tests, the mechanical behavior of materials often differs with the change of strain rates [20, 21]. In regard to material deformation mechanism, apart from the fact that the ideal elastic deformation can be seen as a transient response, other types of inelastic deformations and fractures, such as the diffusion process caused by stress, the evolution process of damage, and the expansion process of cracks, are nontransient responses which are developed at a finite strain rate. Thus, the mechanical properties of the materials are essentially related to the strain rate. It is manifested that with the increase of the strain rate, the yield limit and ultimate strength of materials rise while the elongation declines, and on the contrary, the yield lag and the fracture lag become apparent. Therefore, the correlation between material constitutive equation and strain rate is another reason why the mechanical response of material under impact load differs from that of static loads [22].

The split-Hopkinson pressure bar test is widely adopted as a standard method to measure the dynamic mechanical properties of materials with a strain rate range of $10^{2}s^{-1}$–$10^{4}s^{-1}$ [23]. In this study, the SHPB test was employed to analyze the dynamic mechanical properties of fly ash and lime-stabilized expansive soil.

2. Test Methodology

The soil used in the test is taken from a construction site in Shannan New District, Huainan City, and the physical parameters of the soil samples are measured and shown in Table 1, from which it can be found that the soil belongs to weak expansive soil.

Based on the X-ray diffraction (XRD) tests of fly ash and lime, it indicates that the fly ash is primarily composed of mullite with a small amount of quartz, while the lime mostly contains portlandite with a small amount of vanadium selenide.

In the preparation of samples, the soil was first pulverized through a 0.5 mm sieve. The contents of fly ash were 0% (plain soil), 10%, 20%, and 30% (mass ratio to dry soil) in the first group, respectively. In the second group, 5% lime (mass ratio to dry soil) was added to each sample based on the first group. Cylinder samples with a diameter of 50 mm and a height of 25 mm were made and water content was maintained at 25%. The densities of soil samples are 1.795 g/cm^3 (plain soil), 1.787 g/cm^3 (10% F), 1.787 g/cm^3 (20% F), 1.784 g/cm^3 (30% F), 1.561 g/cm^3 (10% F + 5% L), 1.551 g/cm^3 (20% F + 5% L), and 1.536 g/cm^3 (30% F + 5% L), respectively. The prepared samples were placed in a standard curing box and maintained at 95% relative humidity for 28 days.

For the impact test, a Φ50 mm SHPB test device was used, which consists of a loading system, a striker bar, an incident bar, a transmitted bar, and a signal acquisition system, as shown in Figure 1.

The length of the striker bar, incident bar, and transmitted bar is 0.60 m, 2.40 m, and 1.20 m, respectively. Each bar is made of alloy steel with a density of 7.8 g/cm^3, an elastic modulus of 210 GPa, and a longitudinal wave velocity of 5190 m/s. Considering the low wave impedance of the soil samples, a semiconductor strain gauge was used to collect the voltage signal on the transmitted bar. The DPO3024 digital oscilloscope and KD6009 strain amplifier were used for data and signal acquisition. At the same time, the parallel beam and timer were used to measure the speed of the striker bar. Due to the low strength of soil samples, an impact pressure of 0.2 MPa was adopted in the test.

To ensure a uniform stress inside samples, the following two measures were adopted in the SHPB test:

(1) An appropriate amount of Vaseline was applied to the upper and lower surfaces of samples to reduce the friction effect between the samples and the bars [24].

(2) According to relevant research results, when the length-diameter ratio was 0.5, the uniformity of stress inside samples was relatively good. Therefore, the size of 50 mm × 25 mm was selected [25].

The plain soil and 10% F + 5% L stabilized soil were selected to be two representative soil samples for the analysis of the microstructures. Under a FlexSEM1000 machine, the microstructures of the plain soil and 10% F + 5% L stabilized soil were investigated. Before the SEM test, the soil samples were first polished and then plated with gold for 120 s for the purpose of enhancing their conductivity. The acceleration voltage of SEM analysis was set to 10 kV.

Table 1: Physical parameters of expansive soil.

Moisture content (%)	Density (g/cm$^{3)}$	Dry density (g/cm^3)	Porosity (%)	Void ratio	Plasticity index	Free swelling ratio (%)	Unloading swelling ratio (%)
24.1	1.98	1.60	41.5	0.711	24.91	59.4	13.13

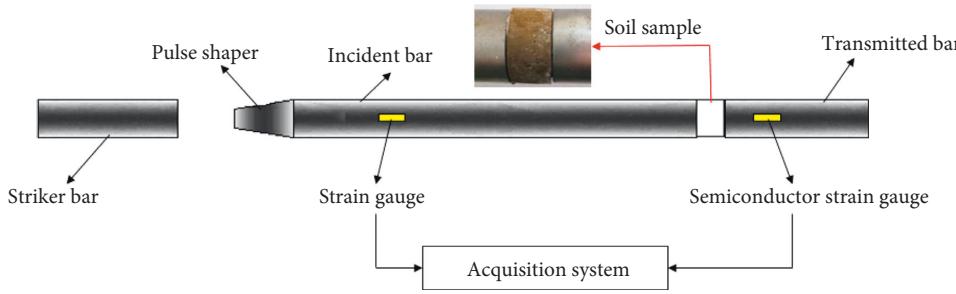

Figure 1: Schematic diagram of the SHPB test device.

3. Test Results

3.1. Dynamic Compressive Strength Analysis. Figure 2 shows the typical shaped waveforms of incident, reflected, and transmitted pulse in the SHPB test.

The dynamic compressive strain and stress in the SHPB test can be calculated with the two-wave method. The relevant formula is as follows [26]:

$$\varepsilon_s(t) = \frac{2c}{L_0}\int_0^t \varepsilon_R(t)\mathrm{d}t,$$
$$\sigma_s(t) = \frac{AE}{A_0}\varepsilon_T(t), \quad (1)$$

where E, c, and A refer to the elastic modulus, longitudinal wave velocity, and cross-sectional area of the bars, respectively; L_0 and A_0 denote the length and cross-sectional area of soil samples, respectively; and $\varepsilon_R(t)$ and $\varepsilon_T(t)$ are the reflected and transmitted pulses, respectively.

The dynamic compressive stress-strain curves of the stabilized expansive soil with different mix proportions are shown in Figure 3. As is shown, the strength of the expansive soil stabilized by both fly ash and lime is significantly higher than that by pure fly ash. The strength of plain soil and pure fly ash-stabilized soil rises firstly and then gradually declines after reaching the peak value. Then a yield platform appears, showing obvious characteristics of plastic failure. After lime is added, the strength of the stabilized soil reaches the peak value and then decreases rapidly, indicating a typical brittle failure. The corresponding dynamic compressive strength is shown in Figure 4. When fly ash is added separately, the strength of the stabilized soil first increases and then decreases with the upregulation of fly ash content. The strength of the stabilized soil reaches the peak value of 713.58 kPa when 20% F is added, which increases by 47.9% compared with that of plain soil (480.02 kPa). This is because the pozzolanic reaction of fly ash tends to produce certain hydration products, which contribute to improving the strength of the stabilized soil within a certain range of fly ash content (0%–20% F). Nevertheless, as a type of fine spherical particles, fly ash is only possessed of a low strength, and too much content will inevitably lead to uneven mixture and agglomeration in the soil, consequently generating a weak surface of direct contact between fly ash particles. Once subjected to an external load, the weak surface first breaks, which in turn reduces the strength of the soil samples. With the addition of lime, the change law of stabilized soil strength exhibits the same regularity, reaching the peak value of 1668.75 kPa at 20% F + 5% F content, with an increase of 247.9% compared with that of plain soil. The results show that lime can significantly promote the hydration reaction in stabilized soil so as to dramatically improve the dynamic compressive strength.

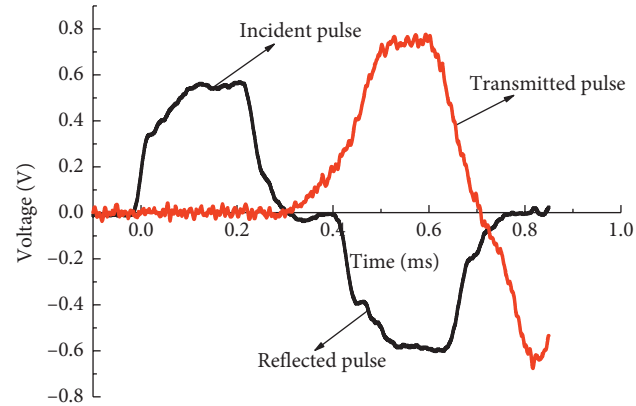

Figure 2: Typical shaped waveforms.

3.2. Energy Dissipation Analysis. From the perspective of thermodynamics, the essence of failure is the process of energy conversion. The failure process of materials always exchanges energy with the outside world. Macroscopic fracture is the final outcome of the continuous aggregation and development of microcracks inside. Thus, the process from microscopic damage to macroscopic failure is accompanied by the dissipation of energy [27]. In the final analysis, material failure refers to a state instability

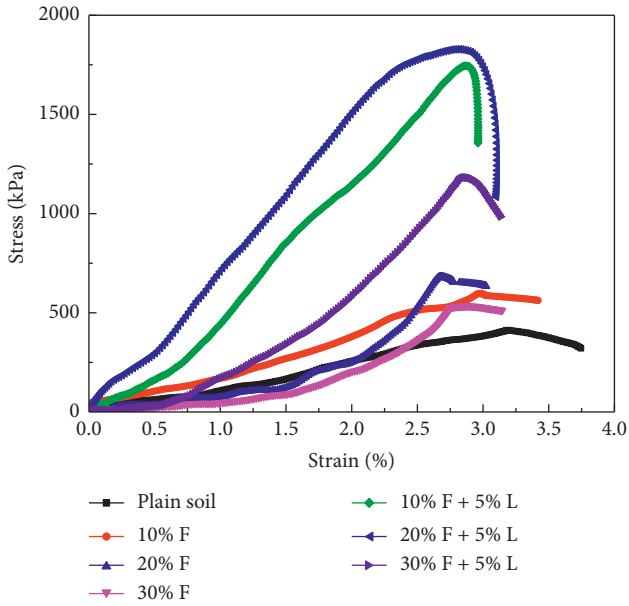

Figure 3: Dynamic compressive stress-strain curves of stabilized soil with different mix proportions.

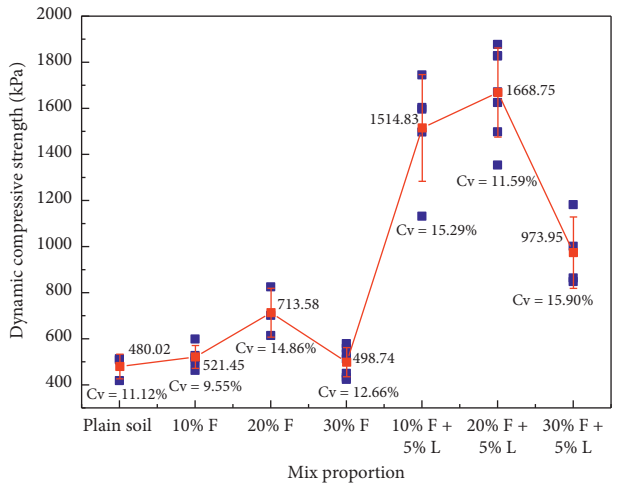

Figure 4: Dynamic compressive strength of stabilized soil with different mix proportions.

phenomenon driven by energy. Therefore, to clarify the failure mechanism of rock and soil, it is of vital importance to analyze energy dissipation.

Under the action of dynamic impact load, energy is the prime force that runs through the whole process of soil deformation and failure. The soil is a typical heterogeneous material with a great many cracks and pores inside. Under the static load, the soil sample has stress concentration at these defects, which then goes through the process of crack propagation to lead the failure. Under the dynamic impact load, on account of the short action time, the strain rate presents to be high, and the internal cracks of soil are too fast to expand in a regular manner. Therefore, the soil sample exhibits irregular and comminuted failure at the macroscopic level. In consequence, its failure process, failure mode, and energy dissipation rules all seem to show great differences from that under static load. Thus, studying the energy dissipation process of the stabilized soil is conducive to revealing the failure mechanism of the soil sample. The calculation formula of the absorbed energy $W_s(t)$ in SHPB test is as follows [28]:

$$W_s(t) = W_I(t) - W_R(t) - W_T(t), \tag{2}$$

where $W_I(t)$, $W_R(t)$, and $W_T(t)$ refer to the energy of incident, reflected, and transmitted pulses, respectively. Based on the assumption of one-dimensional stress wave and the law of energy conservation, the energy of incident, reflected, and transmitted pulses in the SHPB test can be calculated with the following formula:

$$W_i(t) = \frac{Ac}{E}\int \sigma_i^2(t)\mathrm{d}t = EAC\int \varepsilon_i^2(t)\mathrm{d}t, \quad i = \mathrm{I, R, T}. \tag{3}$$

The absorbed energy W_s is mainly composed of three parts: (1) energy consumption for crushing, which is mainly used to generate new fractures and microcracks in the fragments; (2) kinetic energy of fragments ejection; (3) other kinds of energy, which mainly refer to energy dissipated in other different forms like heat [22].

Due to the low wave impedance of stabilized soil, there is little difference between the incident and reflected pulses, the error of absorbed energy calculated by the above formula is large [29]. To avoid this phenomenon, the strain uniformity assumption $\varepsilon_T(t) = \varepsilon_I(t) + \varepsilon_R(t)$ is quoted here, with which the above formula can be changed to

$$\begin{aligned} W_s(t) &= W_I(t) - [W_R(t) + W_T(t)] \\ &= \frac{Ac}{E}\left(\int \sigma_I^2\mathrm{d}t - \int \sigma_R^2\mathrm{d}t - \int \sigma_T^2\mathrm{d}t\right) \\ &= \frac{Ac}{E}\left[\int (\sigma_T - \sigma_R)^2\mathrm{d}t - \int \sigma_R^2\mathrm{d}t - \int \sigma_T^2\mathrm{d}t\right] \\ &= \frac{Ac}{E}\left[\int \left(\sigma_T^2 + \sigma_R^2 - 2\sigma_T\sigma_R\right)\mathrm{d}t - \int \sigma_R^2\mathrm{d}t - \int \sigma_T^2\mathrm{d}t\right] \\ &= -\frac{Ac}{E}\int 2\sigma_T\sigma_R\mathrm{d}t. \end{aligned} \tag{4}$$

Figure 5 shows the variation of incident energy and absorbed energy over time in SHPB test. In the initial stage, the incident energy and the absorbed energy increase with time and remain unchanged after reaching a certain time. Then, the energy does not increase any more, and the absorbed energy only accounts for a small part of the total incident energy.

Figure 6 shows the time-history curves of absorbed energy for stabilized soil with different mix proportions. All the curves show a consistent change law, in which the absorbed energy gradually rises with time and then remains stable. After reaching a stable state, the absorbed energy of soil stabilized by both fly ash and lime presents to be

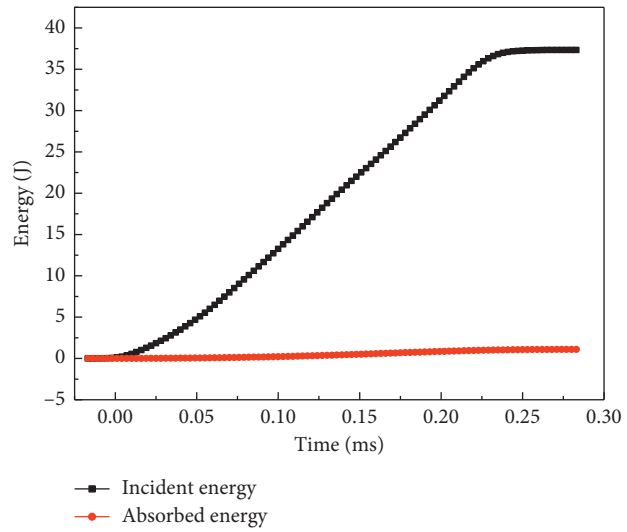

Figure 5: Curves of incident energy and absorbed energy over time in the SHPB test.

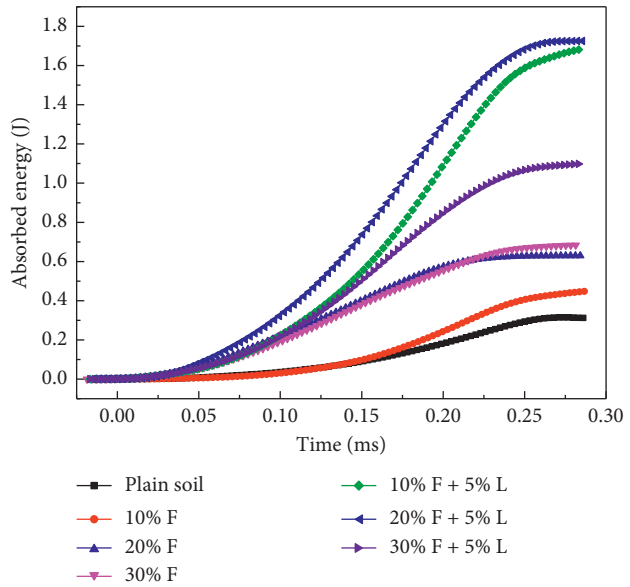

Figure 6: Time-history curves of absorbed energy for stabilized soil with different mix proportions.

significantly higher than that of pure fly ash-stabilized soil and plain soil. The absorbed energy curves of the stabilized soil with different mix proportions are shown in Figure 7.

In order to further clarify the energy dissipation law in the SHPB test, Table 2 shows the incident energy, absorbed energy, and the energy absorbency rate to incident energy under different mix proportions. After the addition of lime, an increase is seen in both the absorbed energy and the energy absorbency rate.

Figure 8 shows the fitted curve of dynamic compressive strength and absorbed energy of stabilized soil. There is a strong positive correlation between dynamic compressive strength and absorbed energy. The greater the sample strength, the more the absorbed energy when failure occurs. The experimental data further prove the correctness of the energy analysis theory.

Table 2: Test results of the energy distribution of soil under different mix proportions.

Specimen number	Incident energy (J)	Absorbed energy (J)	
		Value (J)	Percentage
Plain soil	48.63	0.31	0.64
10% F-1	33.01	0.38	1.15
10% F-2	34.28	0.34	0.99
10% F-3	34.26	0.45	1.31
10% F-4	44.87	0.55	1.23
10% F-5	43.76	0.61	1.39
20% F-1	36.38	0.75	2.06
20% F-2	37.26	0.58	1.56
20% F-3	37.04	0.63	1.70
30% F-1	36.23	0.84	2.32
30% F-2	36.66	0.68	1.85
30% F-3	36.54	0.52	1.42
10% F + 5% L-1	47.19	1.86	3.94
10% F + 5% L-2	40.13	1.14	2.84
10% F + 5% L-3	36.07	1.68	4.66
10% F + 5% L-4	33.74	1.13	3.35
20% F + 5% L-1	48.56	1.33	2.74
20% F + 5% L-2	47.34	1.73	3.65
20% F + 5% L-3	47.91	1.88	3.92
20% F + 5% L-4	44.47	1.58	3.55
20% F + 5% L-5	39.6	1.92	4.85
20% F + 5% L-6	33.91	1.58	4.66
30% F + 5% L-1	46.87	0.75	1.60
30% F + 5% L-2	37.34	1.1	2.95
30% F + 5% L-3	42.4	1.08	2.55
30% F + 5% L-4	33.61	0.78	2.32

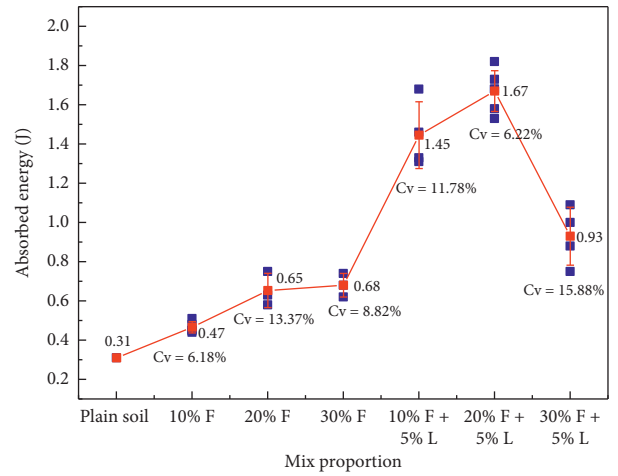

Figure 7: Absorbed energy curve of soil under different mix proportions.

3.3. Fracture Morphology Analysis. In the SHPB test, the fracture morphology of stabilized soil under different mix proportions is shown in Figure 9. It can be seen that due to the strong plasticity of plain soil and pure fly ash-stabilized soil, the soil samples under the impact load exhibit good integrity, except for some cracks and a small amount of fracture gaps. After the addition of lime, the periphery of soil samples is mostly small-scale fragments, and even pulverization occurs; the samples are broken obviously.

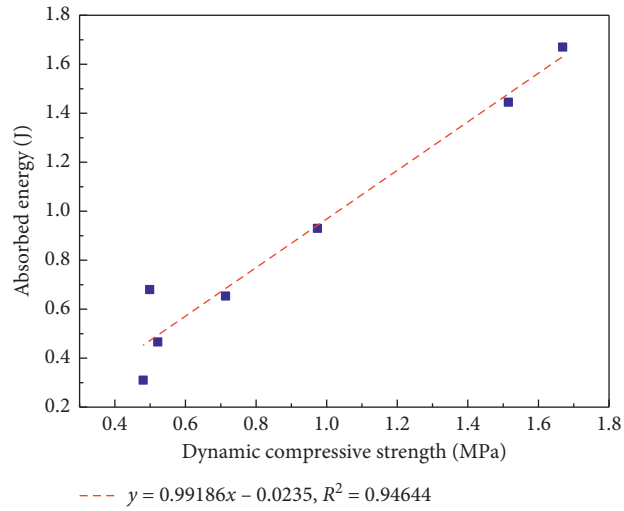

Figure 8: Fitted curve of dynamic compressive strength and absorbed energy.

The evolution of soil samples from microscopic damage to macroscopic fractures is a fractal process. The geometric characteristics of structural evolution and the numerical characteristics of physical-mechanical properties both show good statistical self-similarity. Due to the large degree of fragment distribution and the large span of different fragment sizes, in order to give a visual description of the distribution for the broken fragments of stabilized soil after failure, a standard sieve was used to screen the broken fragments. The average size D of the broken fragments was used to indicate the damage degree of the stabilized soil [30]. As shown in formula (5), the corresponding screening results are shown in Table 3 (considering the high integrity of plain soil and pure fly ash-stabilized soil, it is of little significance to analyze the fracture morphology from the perspective of the fractal theory. Thus, only the fractal characteristic of fly ash-lime combined stabilized soil is discussed here):

$$D = \frac{\sum_{i=1}^{10} r_i d_i}{\sum_{i=1}^{10} r_i}, \tag{5}$$

where d_i refers to the average of the largest particle size and the smallest particle size in each screening particle size range, mm, and r_i refers to the percentage of the fragment mass corresponding to d_i in the total mass M.

In 1975, the mathematician B. B. Mandelbort proposed the fractal theory to reveal the phenomenon, which was irregular but showed self-similarity. Under impact load, the fly ash-lime combined stabilized soil exhibits an obvious form of disorder, which can be regarded as an uncertain system. Therefore, fractal theory is likely to explain some inherent laws hidden in this complex phenomenon [30].

Based on the G-G-S distribution and the mass-frequency relationship [31], the equation for the fragmentation degree of stabilized soil is

$$y = \frac{m_r}{m_T} = \left(\frac{r}{r_m}\right)^b, \tag{6}$$

where r is the particle size of fragments, mm; r_m is the maximum particle size of fragments, mm; m_r is the cumulative mass of fragments with a smaller particle size than r, g; m_T is the total mass of the fragments, g; and b is the distribution parameter, which is equal to the slope of $\ln[m_r/m_T] - \ln[r/r^m]$ curve. Define the fractal dimension D_b:

$$D_b = \log_r N^{-1}, \tag{7}$$

where N stands for the number of fragments with a particle size larger than r. Considering the relationship between N and m, i.e., $d_m \propto r^3 dN$, the fractal dimension D_b can be acquired with the mass-particle method, i.e., $b = (3 - D_b)$, which is equal to the slope of the $\ln[m_r/m_T] - \ln[r/r^m]$ curve. A large fractal dimension means more fragments of the sample, a smaller fragment size, and a larger fragmentation degree [29, 30].

Figure 10 shows the $\ln[m_r/m_T] - \ln[r/r^m]$ curve of the fly ash-lime combined stabilized soil in the SHPB test. The good linear correlation of the test data on the coordinate axes indicates that the fragmentation distribution of the stabilized soil after impact load has good fractal characteristics, which is because the stabilized soil has lots of microcracks and other mesoscopic damages inside. There is self-similarity among them within a certain range, and the failure process and fragment morphology are caused by the evolution of internal damage. Under such circumstances, the distribution of fragmentation can be considered as a statistical fractal.

Figure 11 shows the fitted curve of fractal dimension and absorbed energy. In the SHPB test, the fractal dimension of 10% F + 5% L, 20% F + 5% L, and 30% F + 5% L stabilized soil is 2.4177, 2.2957, and 2.5033, respectively. The absorbed energy of soil samples gradually decreases within the fractal dimension range of 2.3–2.5. Based on the results above, it is shown that a reasonable amount of fly ash and lime content has a positive effect on the fracture morphology of the stabilized soil. Under the condition of 20% F + 5% L content, the stabilized soil exhibits the highest dynamic compressive strength and absorbed energy but the smallest fractal dimension, which indicates that the fragment size is relatively large after the soil sample is broken. The hydration product of the modifier inhibits the expansion of the damage cracks to some extent. In conclusion, 20% F + 5% L proves to be the optimal mix proportion under the test conditions.

3.4. Microstructures Analysis. SEM, as one of the most important methods to explore the microstructures of soil and rock samples, can be adopted to intuitively display the characteristics of micropore morphology. So far, many scholars have conducted lots of research and analysis on the microscopic pore structures of soil and rock samples by means of SEM images [13, 30, 32], but most of them remain at the level of qualitative identification or morphological description of microstructure, and a lot of quantitative information involved in SEM images have been ignored.

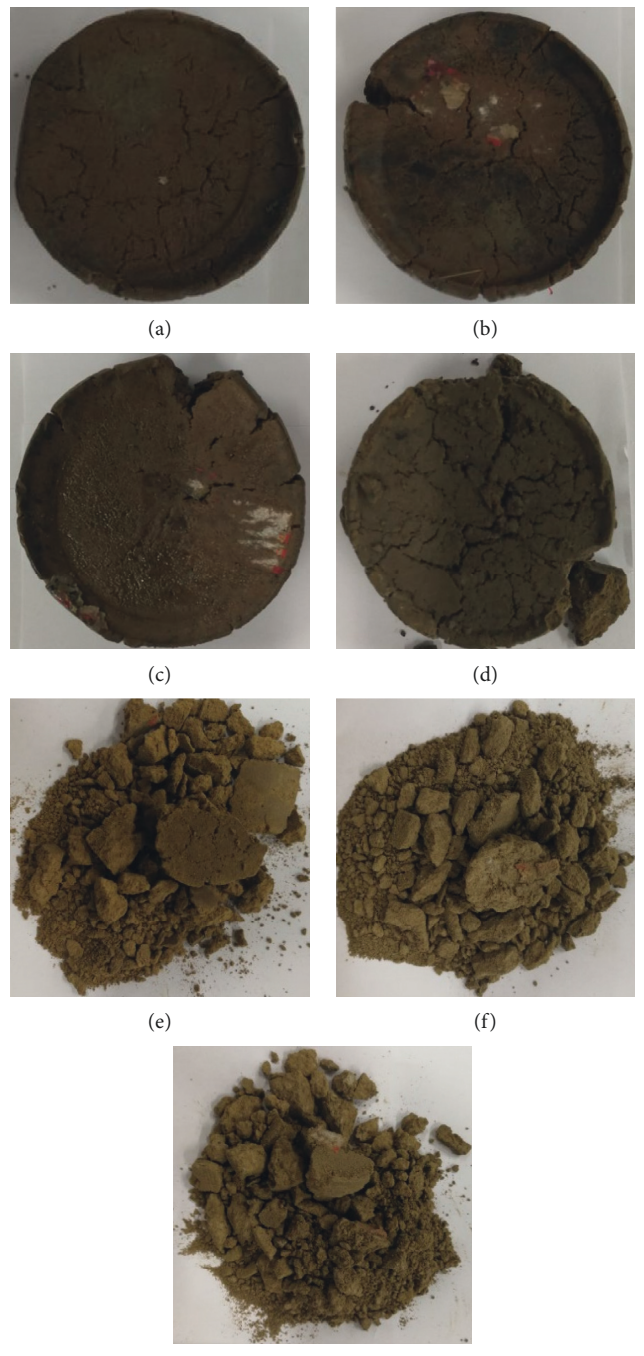

Figure 9: Fracture morphology of stabilized soil under different mix proportions. (a) Plain soil; (b) 10% F stabilized soil; (c) 20% F stabilized soil; (d) 30% F stabilized soil; (e) 10% F + 5% L stabilized soil; (f) 20% F + 5% L stabilized soil; (g) 30% F + 5% L stabilized soil.

Table 3: Screening results of impact fragments of stabilized soil in the SHPB test.

Sample types	Screening particle size (mm)										M (g)	D (mm)
	0	0.1	0.25	0.5	1	2	5	10	30	50		
10% F + 5% L	0.16	3.86	4.48	5.3	4.72	18.48	17.26	25.22	19.22	0	98.70	14.99
20% F + 5% L	0.06	2.49	3.44	4.46	4.07	17.20	16.43	24.37	27.29	0	99.80	17.75
30% F + 5% L	0	5.84	5.76	6.68	4.88	18.86	15.92	19.88	12.92	0	90.74	12.86

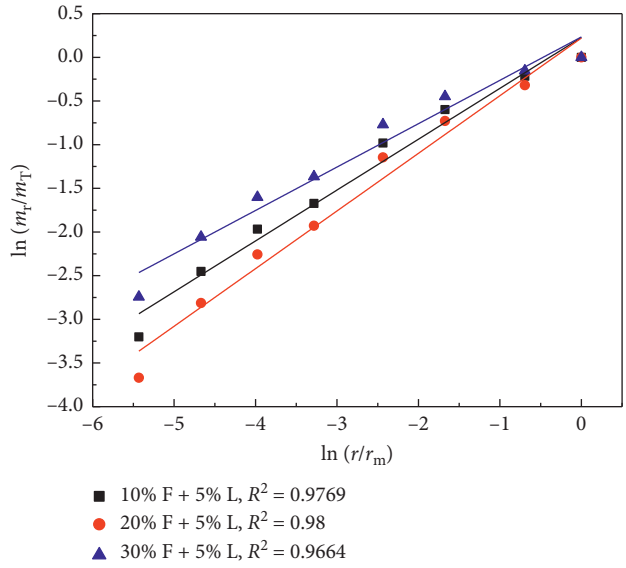

Figure 10: The $\ln[m_r/m_T] - \ln[r/r^m]$ curve in the SHPB test.

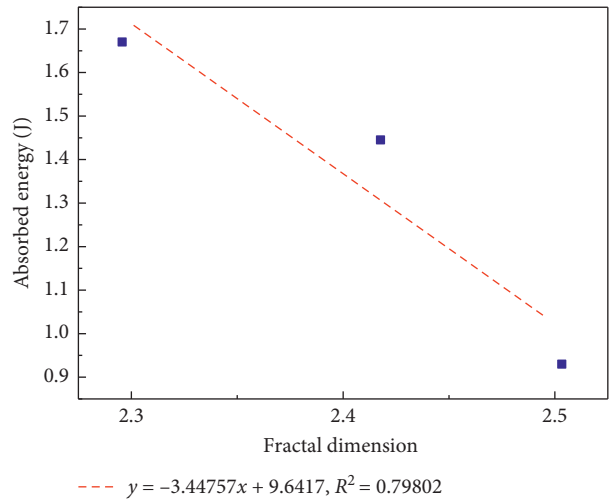

Figure 11: Fitted curve of fractal dimension and absorbed energy of stabilized soil.

Fractal theory is adopted not only to quantitatively characterize the morphology and distribution features of complex objects but also to characterize the pore diameter distribution as well as particle morphology of rocks and soil mass. With SEM images, it is possible to clearly show the pore characteristics of both plain soil and stabilized soil. Suppose there are fractal characteristics in the pore morphology, the relationship between pore perimeter and area is as follows [33, 34]:

$$\lg P = \frac{D}{2}\lg A + C, \tag{8}$$

where P is the perimeter of pores extracted by SEM images, nm; A is the area, nm^2; D is the fractal dimension of pore morphology; and C is a constant.

To quantitatively characterize the microscopic pore characteristics, a professional graphics processing software image J was used to binarize the SEM images and extract the shape of pores and cracks, and the schematic diagram is given in Figure 12.

Under different magnification multiples (×100, ×1000) by means of setting a specific gray threshold, the original and binarization SEM images are shown in Figure 13.

According to equation (8), the pore area and perimeter were fitted linearly. As shown in Figure 14, there is a good linear relationship in the logarithmic coordinate of the pore area and the perimeter of plain soil and stabilized soil, indicating that the pore morphology possesses good fractal characteristics. Based on the fractal principle, the larger the fractal dimension is, the more complex the pore morphology is; the smaller the fractal dimension of pores is, the simpler the pore morphology is, and the closer it is to a circle [33].

It can be seen that the fractal dimension of the pores in plain soil is 2.544–2.550, which is less than that of 10% F + 5% L stabilized soil (2.628–2.658) under the condition of 100 times of magnification (×100). Under the 1000 times of magnification,

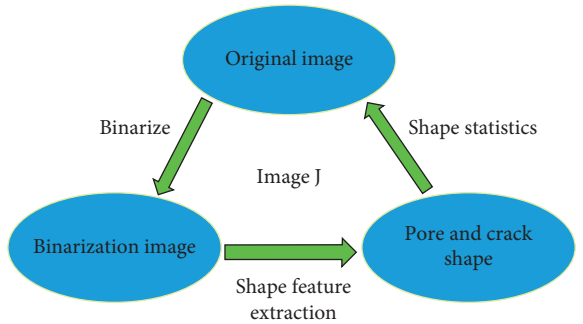

Figure 12: Schematic diagram of pore and crack shape extraction.

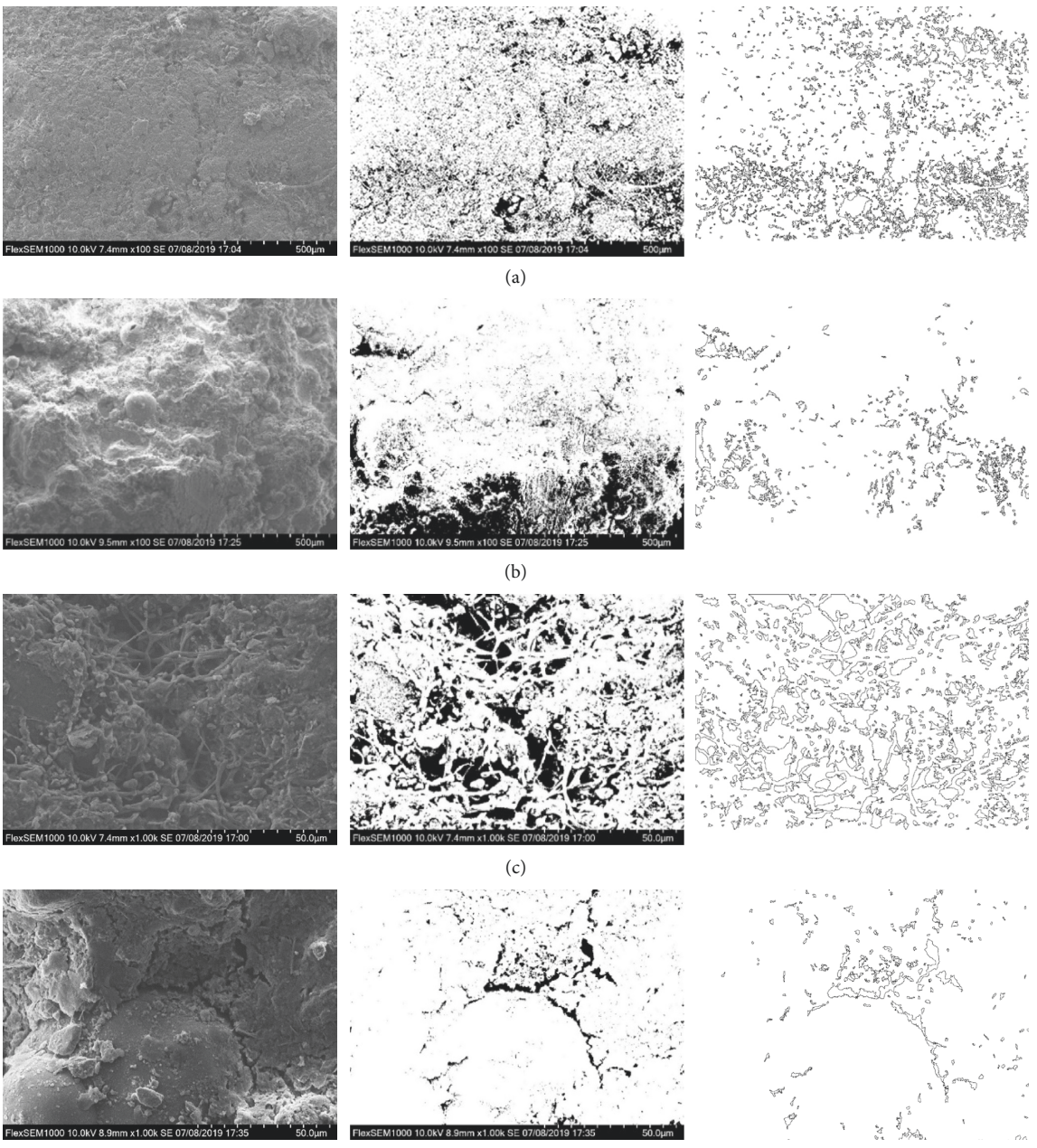

Figure 13: Original and binarization SEM images. (a) Plain soil (×100); (b) 10% F + 5% L stabilized soil (×100); (c) plain soil (x1000); (d) 10% F + 5% L stabilized soil (×1000).

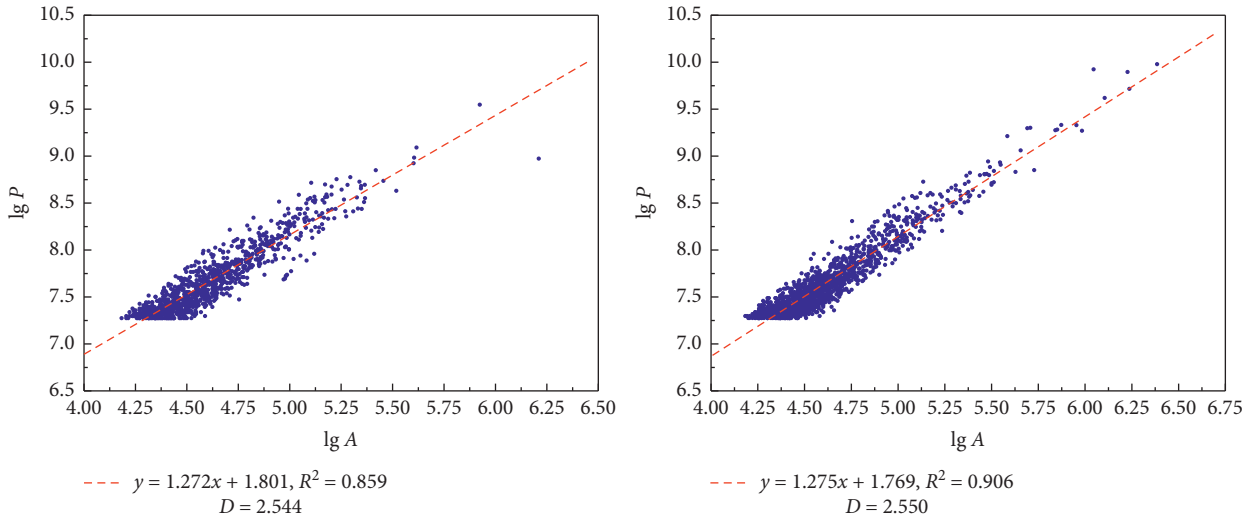

(a)

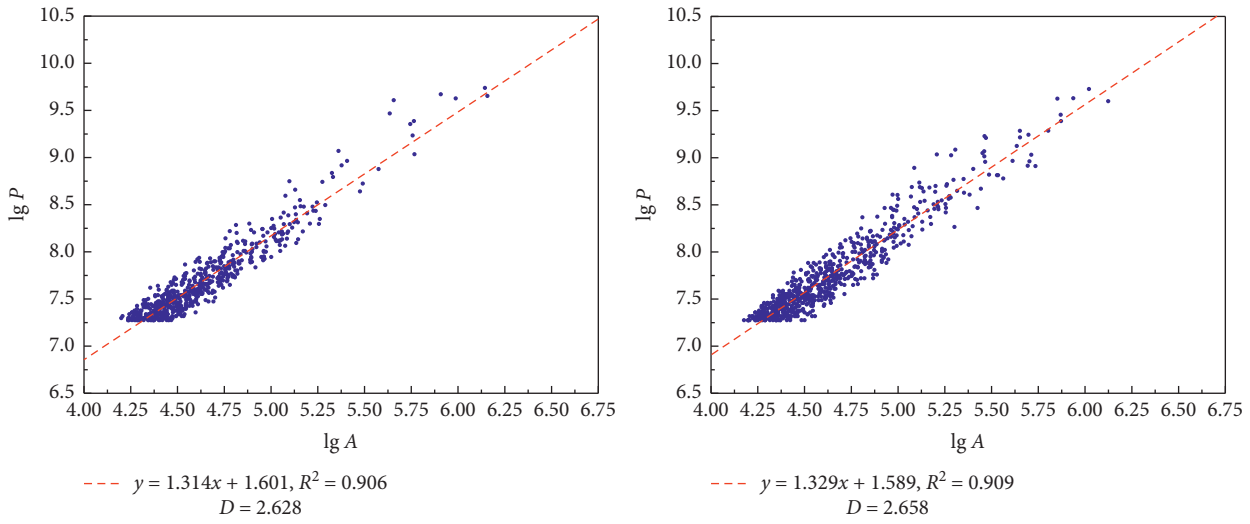

(b)

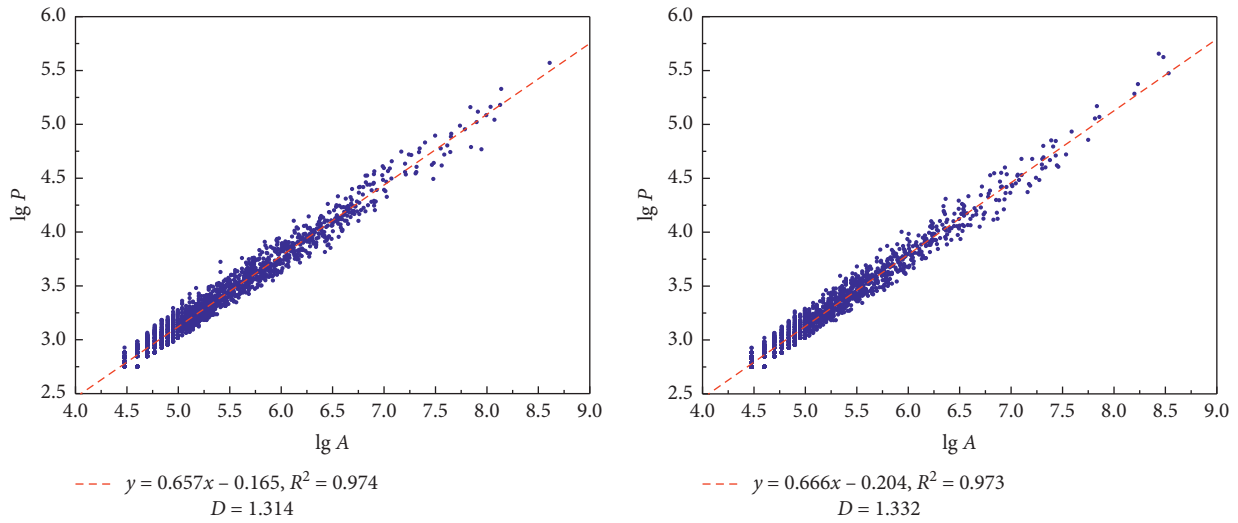

(c)

Figure 14: Continued.

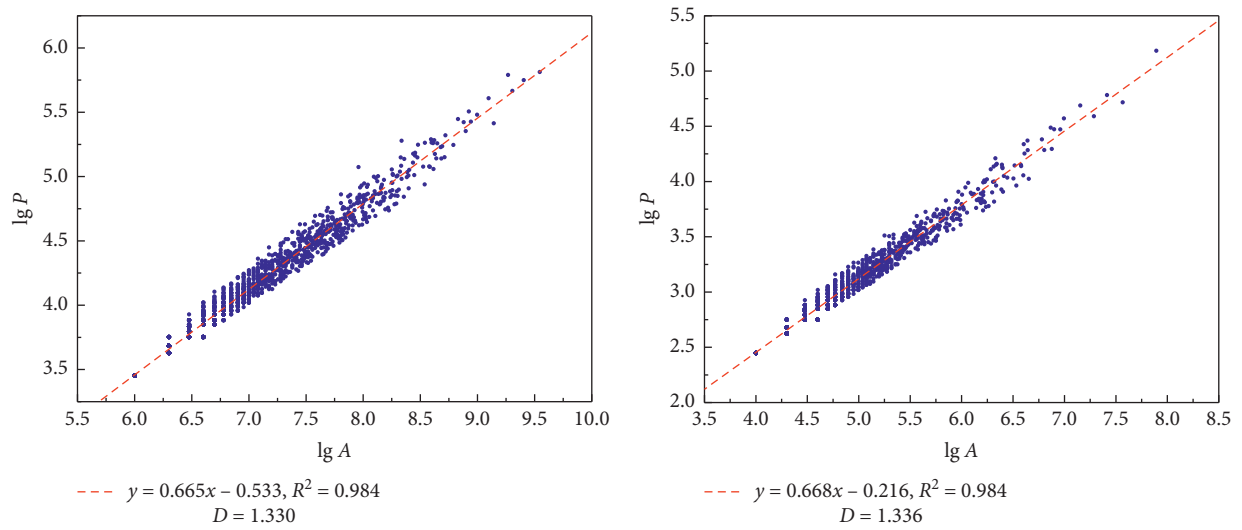

(d)

Figure 14: Fitted curve of fractal dimension of pore morphology. (a) Plain soil (×100); (b) 10% F + 5% L stabilized soil (×100); (c) plain soil (×1000); (d) 10% F + 5% L stabilized soil (×1000).

the fractal dimension of the pores in plain soil is 1.314 (another set of data is 1.332, and this is because the soil surface contains a more flake thin layer structure, and the overlaps in SEM images is serious, causing that the pores on the surface of the soil sample are shielded to some extent. Therefore, the complete pores are divided into complex and irregular shapes, which is not considered here), less than that of 10% F + 5% L stabilized soil (1.330–1.336). This phenomenon indicates that the internal pore morphology of plain soil is relatively simple, which is close to the shape of a circle. However, this pore structure is filled with the hydration products of the modifier to some extent, which transforms the pore morphology of stabilized soil into irregular and small cracks. Consequently, the compactness and integrity of the soil are further improved.

4. Conclusion

In this study, an analysis was made on the dynamic mechanical properties and energy dissipation law of fly ash and lime-stabilized expansive soil based on the SHPB test. Both the relationship between dynamic compressive strength and absorbed energy and the relationship between fractal dimension and absorbed energy were obtained. The microstructures of plain soil and stabilized soil were analyzed by SEM images. Relevant research conclusions are as follows:

(1) The dynamic compressive strength and absorbed energy of the stabilized soil first increase and then decrease with the rise of fly ash and lime content and finally reach the peak value under the mix proportion of 20% F + 5% L, which is 1670 kPa and 1.67 J, respectively. More than the addition of 20% F + 5% L, the dynamic compressive strength and absorbed energy are reduced because of the presence of the weak surface of fly ash-fly ash particles. Due to the low wave impedance of the soil, the absorbed energy in the test only accounts for a very small part of the incident energy.

(2) The dynamic compressive strength of the stabilized soil has a good linear relationship with the absorbed energy. The greater the strength, the more the absorbed energy after the failure of soil. The failure mechanism of the soil samples under impact load is well analyzed from the perspective of energy dissipation.

(3) The fracture morphology of fly ash-lime combined stabilized soil presents significant differences from that of plain soil and pure fly ash-stabilized soil. Under the impact load of 0.2 MPa, the integrity of plain soil and pure fly ash-stabilized soil is relatively good, while the soil stabilized by both fly ash and lime shows comminuted failure. The absorbed energy gradually declines within the range of fractal dimension from 2.30 to 2.50. It shows that a reasonable amount of modifier has a certain positive effect on the failure fracture characteristics of soil. According to the test results, the modifier content of 20% F + 5% L proves to be the optimal mix proportion.

(4) The fractal dimension of pore morphology obtained from the binarization of SEM images is able to quantitatively characterize the pore morphology characteristics of plain soil and stabilized soil. The microstructure of plain soil differs from that of fly ash-lime combined stabilized soil. The pores of plain soil are much closer to the shape of a circle. In contrast, the fracture morphology of stabilized soil tends to be slender and irregular microcracks. Therefore, the stabilized soil is of better compactness and higher strength.

Data Availability

The data used to support the findings of this study are available from the corresponding author upon request.

Conflicts of Interest

The authors declare that they have no conflicts of interest regarding the publication of this paper.

Acknowledgments

This work was supported by the Major Universities Natural Science Research Project in Anhui Province (KJ2016SD19), the National Natural Science Foundation of China (41977236, 41672278, and 41271071), and Natural Science Foundation of Jiangxi Province (2019ACBL20002). The authors sincerely thank the School of Civil Engineering and Architecture, National Engineering Laboratory for Deep Shaft Construction Technology in Coal Mine in Anhui University of Science and Technology for providing the experiment conditions.

References

[1] J. Li, D. A. Cameron, and G. Ren, "Case study and back analysis of a residential building damaged by expansive soils," *Computers and Geotechnics*, vol. 56, pp. 89–99, 2014.

[2] H. H. Adem and S. K. Vanapalli, "Constitutive modeling approach for estimating1-Dheave with respect to time for expansive soils," *International Journal of Geotechnical Engineering*, vol. 7, no. 2, pp. 199–204, 2013.

[3] T. M. Petry and D. N. Little, "Review of stabilization of clays and expansive soils in pavements and lightly loaded structures-history, practice, and future," *Journal of Materials in Civil Engineering*, vol. 14, no. 6, pp. 447–460, 2002.

[4] C. M. O. Nwaiwu and I. Nuhu, "Evaluation and prediction of the swelling characteristics of Nigerian black clays," *Geotechnical and Geological Engineering*, vol. 24, no. 1, pp. 45–56, 2006.

[5] A. R. Estabragh, M. Moghadas, and A. A. Javadi, "Effect of different types of wetting fluids on the behaviour of expansive soil during wetting and drying," *Soils and Foundations*, vol. 53, no. 5, pp. 617–627, 2013.

[6] H. H. Adem and S. K. Vanapalli, "Review of methods for predicting in situ volume change movement of expansive soil over time," *Journal of Rock Mechanics and Geotechnical Engineering*, vol. 7, no. 1, pp. 73–86, 2015.

[7] H. Elbadry, "Simplified reliable prediction method for determining the volume change of expansive soils based on simply physical tests," *HBRC Journal*, vol. 13, no. 3, pp. 353–360, 2017.

[8] P. VenkaraMuthyalu, K. Ramu, and G. V. R. Prasada Raju, "Study on performance of chemically stabilized expansive soil," *International Journal of Advances in Engineering &Technology*, vol. 2, no. 1, pp. 139–148, 2012.

[9] H. Zhao, K. Zhou, C. Zhao, B.-W. Gong, and J. Liu, "A long-term investigation on microstructure of cement-stabilized handan clay," *European Journal of Environmental and Civil Engineering*, vol. 20, no. 2, pp. 199–214, 2016.

[10] R. N. Yong and V. R. Ouhadi, "Experimental study on instability of bases on natural and lime/cement-stabilized clayey soils," *Applied Clay Science*, vol. 35, no. 3-4, pp. 238–249, 2007.

[11] A. S. Rao and M. R. Rao, "Swell-shrink behaviour of expansive soils under stabilized fly ash cushions," in *Proceedings of the 12th International Conference on International Association for Computer Methods and Advances in Geomechanics*, pp. 561–564, Goa, India, December 2008.

[12] A. K. B. S. Walia and A. Bajaj, "Influence of fly ash, lime, and polyester fibers on compaction and strength properties of expansive soil," *Journal of Materials in Civil Engineering*, vol. 19, no. 3, pp. 242–248, 2007.

[13] Q.-Y. Ma, Z.-M. Cao, and P. Yuan, "Experimental research on microstructure and physical-mechanical properties of expansive soil stabilized with fly ash, sand, and basalt fiber," *Advances in Materials Science and Engineering*, vol. 2018, Article ID 9125127, 13 pages, 2018.

[14] S. K. Dash and M. Hussain, "Lime stabilization of soils: reappraisal," *Journal of Materials in Civil Engineering*, vol. 24, no. 6, pp. 707–714, 2012.

[15] A. K. Sabat, "A study on some geotechnical properties of lime stabilized expansive soil-quarry dust mixes," *International Journal of Emerging Trends in Engineering and Development*, vol. 1, no. 2, pp. 42–49, 2012.

[16] M. R. Thompson, "Lime reactivity of Illinois soils," *Journal of the Soil Mechanics and Foundation Division*, vol. 92, no. 5, pp. 67–92, 1966.

[17] V. R. Ouhadi and R. N. Yong, "The role of clay fraction of marly soil on their post stabilization failure," *Engineering Geology*, vol. 70, no. 3-4, pp. 365–375, 2003.

[18] M.-M. Qiu, G.-L. Yang, Q. Shen, X. Yang, G. Wang, and Y.-L. Lin, "Dynamic behavior of new cutting subgrade structure of expensive soil under train loads coupling with service environment," *Journal of Central South University*, vol. 24, no. 4, pp. 875–890, 2017.

[19] X. Li, Q. G. Cheng, J. C. Zhang, and Y. Yao, "Experimental study on dynamic performance of cement-improved expansive soil in high speed railway subgrade in wetting-drying cycles," *Railway Engineering*, vol. 2016, no. 6, pp. 99–103, 2016.

[20] D. L. Grote, S. W. Park, and M. Zhou, "Dynamic behavior of concrete at high strain rates and pressures: I. experimental characterization," *International Journal of Impact Engineering*, vol. 25, no. 9, pp. 869–886, 2001.

[21] J.-K. Zhou and L.-M. Ge, "Effect of strain rate and water-to-cement ratio on compressive mechanical behavior of cement mortar," *Journal of Central South University*, vol. 22, no. 3, pp. 1087–1095, 2015.

[22] L. Hong, *Size effect on strength and energy dissipation in fracture of rock under impact loads*, Ph.D. thesis, Central South University, Changsha, China, 2008.

[23] J. E. Field, S. M. Walley, W. G. Proud, H. T. Goldrein, and C. R. Siviour, "Review of experimental techniques for high rate deformation and shock studies," *International Journal of Impact Engineering*, vol. 30, no. 7, pp. 725–775, 2004.

[24] L. Hong, Z.-L. Zhou, T.-B. Yin, G.-Y. Liao, and Z.-Y. Ye, "Energy consumption in rock fragmentation at intermediate strain rate," *Journal of Central South University of Technology*, vol. 16, no. 4, pp. 677–682, 2009.

[25] Y. X. Zhou, K. Xia, X. B. Li et al., "Suggested methods for determining the dynamic strength parameters and mode-I fracture toughness of rock materials," *International Journal of Rock Mechanics and Mining Sciences*, vol. 49, pp. 105–112, 2012.

[26] L. Song and S. S. Hu, "Two-wave and three-wave method in SHPB data processing," *Explosion and Shock Waves*, vol. 25, no. 4, pp. 368–373, 2005, in Chinese.

[27] D. N. Whittles, S. Kingman, I. Lowndes, and K. Jackson, "Laboratory and numerical investigation into the

characteristics of rock fragmentation," *Minerals Engineering*, vol. 19, no. 14, pp. 1418–1429, 2006.

[28] L. L. Cao, H. Pu, M. Li, X.-B. Mao, and L.-Y. Zhang, "Experimental research on the dynamic tensile fracture and the energy dissipation characteristics of coal-serial sandstone," *Journal of China Coal Society*, vol. 42, no. 2, pp. 492–499, 2017, in Chinese.

[29] D. D. Ma, *Study on dynamic mechanical property and constitutive model of artificial frozen soil under coupled static and dynamic load*, Ph.D. thesis, Anhui University of Science and Technology, Huainan, China, 2018.

[30] C. H. Gao, *SHPB test for basalt fiber reinforced cement-soil and its microstructure analysis*, Ph.D. thesis, Anhui University of Science and Technology, Huainan, China, 2018.

[31] H. F. Deng, Z. Wang, J. L. Li et al., "Effect of unloading rate and pore water pressure on mechanical properties of sandstone," *Chinese Journal of Geotechnical Engineering*, vol. 39, no. 11, pp. 1976–1983, 2017, in Chinese.

[32] Y. Xia, H. Zhou, C. Zhang, S. He, Y. Gao, and P. Wang, "The evaluation of rock brittleness and its application: a review study," *European Journal of Environmental and Civil Engineering*, pp. 1–41, 2019.

[33] P. F. Zhang, S. F. Lu, J. Q. Li, H. T. Xue, W. B. Li, and S. Y. Wang, "Quantitative characterization of microscopic pore structure for shales using scanning electron microscopy," *Journal of China University of Petroleum*, vol. 42, no. 2, pp. 19–28, 2018, in Chinese.

[34] B. J. Wang, B. Shi, Z. B. Liu, and Y. Cai, "Fractal study on microstructure of clayey soil by GIS," *Chinese Journal of Geotechnical Engineering*, vol. 26, no. 2, pp. 244–247, 2004, in Chinese.